Chinese Journal of Aeronautics, (2017), 30(5): 1708–1718

Chinese Society of Aeronautics and Astronautics
& Beihang University

Chinese Journal of Aeronautics

cja@buaa.edu.cn
www.sciencedirect.com

Boundary discontinuous Fourier analysis of thick beams with clamped and simply supported edges via CUF

F.G. CANALES [a], J.L. MANTARI [a,b,*]

[a] Faculty of Mechanical Engineering, Universidad de Ingeniería y Tecnología (UTEC), Lima 15063, Peru
[b] Department of Mechanical Engineering, University of New Mexico, Albuquerque 87131, USA

Received 30 June 2016; revised 28 October 2016; accepted 24 January 2017
Available online 11 July 2017

KEYWORDS

Analytical solution;
Beam;
Clamped;
Fourier;
Unified formulation

Abstract This paper presents an analytical solution for static analysis of thick rectangular beams with different boundary conditions. Carrera's Unified Formulation (CUF) is used in order to consider shear deformation theories of arbitrary order. The novelty of the present work is that a boundary discontinuous Fourier approach is used to consider clamped boundary conditions in the analytical solution, unlike Navier-type solutions which are restricted to simply supported beams. Governing equations are obtained by employing the principle of virtual work. The numerical accuracy of results is ascertained by studying the convergence of the solution and comparing the results to those of a 3D finite element solution. Beams subjected to bending due to a uniform pressure load and subjected to torsion due to opposite linear forces are considered. Overall, accurate results close to those of 3D finite element solutions are obtained, which can be used to validate finite element results or other approximate methods.

1. Introduction

1D theories are widely used to analyze behaviors of slender bodies in a computationally efficient manner. For this reason, many beam models have been developed. The most well-known beam theory is the classical or Euler-Bernoulli beam theory, which yields reasonably good results for slender beams. However, this model does not take into account shear deformations in a beam. The Timoshenko beam theory is an improvement over the classical theory that considers a uniform shear distribution across the thickness of a beam. However, this theory requires a shear correction factor to correct the strain energy of deformation. Discussion of shear coefficients has been presented in Refs.[1–4]

A large amount of Higher-order Shear Deformation Theories (HSDTs) have been developed in order to consider a nonuniform shear distribution in a beam's cross-section. HSDTs with polynomial distributions of shear deformation

* Corresponding author.
E-mail address: jmantari@utec.edu.pe (J.L. MANTARI).
Peer review under responsibility of Editorial Committee of CJA.

ELSEVIER Production and hosting by Elsevier

http://dx.doi.org/10.1016/j.cja.2017.06.014

across the thickness are common due to their simplicity, and some have been presented in Refs.[5–13] Theories containing trigonometric functions in thickness coordinates are also common. A trigonometric shear deformation theory has been presented by Dahake and Ghugal.[14] Many polynomial and trigonometric deformation theories have been developed for analysis of laminated beams, as presented in Refs.[15–20] First-order shear deformation theories are popular due to their computational efficiency, and some have been given in Refs.[21–24]

In order to analyze theories with arbitrary order in a systematic manner, a unified formulation known as Carrera's Unified Formulation (CUF) has been developed in Ref.[25] This formulation has been applied to solve multifield problems, as presented in Refs.[26–28] Carrera and Giunta[29] used the 1D-CUF model to analyze 1D problems with complex cross-sections, and further development has been presented by Carrera et al.[30–32] The capability of these models to obtain quasi-3D solutions has been exploited to develop accurate static[33], free vibration[34,35], and buckling analysis[36] of composite beams.

Analytical solutions for bending of simply supported beams are obtained by using a Fourier series in Navier-type solutions. Other boundary conditions such as clamped conditions can be considered in a finite element formulation or by using the Ritz method, but accurate analytical solutions for these boundary conditions are a fairly scarce topic in the literature. Since finite element formulations or variational methods obtain approximate results, exact analytical solutions are required as a benchmark in order to assess the validity of the results. The present work intends to provide such analytical solutions for clamped boundary conditions.

A generalization of the Fourier series method known as the boundary discontinuous Fourier method can take into account clamped boundary conditions. This method was developed by Chaudhuri in Refs.[37,38] Discontinuities are introduced in order to satisfy boundary constraints. This solution methodology has been applied for static and free vibration analysis of cylindrical panels,[39,40] doubly-curved panels,[41–48] and plates.[49–54] Since the rate of convergence of a Fourier series is slower in the presence of discontinuities, a mixed Fourier solution has also been developed in Refs.[55,56] in order to produce accelerated convergence. Oktem and Chaudhuri have applied the boundary discontinuous Fourier method for analysis of plates[57–59] and shells[60–63] using HSDTs.

In this paper, an analytical solution for static analysis of thick beams with Clamped-Clamped (C-C) and Clamped-Simple (C-S) boundary conditions is obtained. A general approach to obtain such an analytical solution using a unified formulation is currently unavailable in the literature, since the other option commonly used for static analysis of beams is a Navier-type solution, which can only consider simply supported edges. Theories of arbitrary order are considered in a systematic manner by using CUF. The principle of virtual work is used to obtain governing equations. The convergence of the solution is analyzed and 3D finite element solutions are obtained in order to assess the validity of results. Good results agreements with 3D finite element solutions are obtained. The results can be used as a benchmark for comparison with approximate solution methods.

2. Analytical modeling

A beam of length L, width b, and total thickness h is considered in the present analysis. The rectangular Cartesian coordinate system used in the present work is shown in Fig. 1. The beam occupies the following region: $-b/2 \leqslant x \leqslant b/2$, $0 \leqslant y \leqslant L$, $-h/2 \leqslant z \leqslant h/2$.

2.1. Elastic stress-strain relations

A general displacement vector is introduced:

$$\boldsymbol{u}(x,y,z) = [\,u_x \quad u_y \quad u_z\,]^{\mathrm{T}} \tag{1}$$

The cross-sectional plane of the beam is denoted by Ω. The stress and strain components are grouped as

$$\begin{cases} \boldsymbol{\sigma}_{\mathrm{p}} = [\,\sigma_{zz} \quad \sigma_{xx} \quad \sigma_{zx}\,]^{\mathrm{T}} \\ \boldsymbol{\varepsilon}_{\mathrm{p}} = [\,\varepsilon_{zz} \quad \varepsilon_{xx} \quad \varepsilon_{zx}\,]^{\mathrm{T}} \\ \boldsymbol{\sigma}_{\mathrm{n}} = [\,\sigma_{zy} \quad \sigma_{xy} \quad \sigma_{yy}\,]^{\mathrm{T}} \\ \boldsymbol{\varepsilon}_{\mathrm{n}} = [\,\varepsilon_{zy} \quad \varepsilon_{xy} \quad \varepsilon_{yy}\,]^{\mathrm{T}} \end{cases} \tag{2}$$

where σ_{ij} and ε_{ij} are the components of the stress and strain vectors, respectively. Subscript "p" stands for terms lying on planes orthogonal to the cross-section, while subscript "n" stands for terms lying on the cross-section. Considering small amplitude displacements, the strain-displacement relations are

$$\begin{cases} \boldsymbol{\varepsilon}_{\mathrm{p}} = \boldsymbol{D}_{\mathrm{p}}\boldsymbol{u} \\ \boldsymbol{\varepsilon}_{\mathrm{n}} = \boldsymbol{D}_{\mathrm{n}}\boldsymbol{u} = (\boldsymbol{D}_{\mathrm{n}\Omega} + \boldsymbol{D}_{\mathrm{n}y})\boldsymbol{u} \end{cases} \tag{3}$$

The linear differential operators $\boldsymbol{D}_{\mathrm{p}}$, $\boldsymbol{D}_{\mathrm{n}\Omega}$, and $\boldsymbol{D}_{\mathrm{n}y}$ are given by

$$\begin{cases} \boldsymbol{D}_{\mathrm{p}} = \begin{bmatrix} 0 & 0 & \dfrac{\partial}{\partial z} \\ \dfrac{\partial}{\partial x} & 0 & 0 \\ \dfrac{\partial}{\partial z} & 0 & \dfrac{\partial}{\partial x} \end{bmatrix} \\ \boldsymbol{D}_{\mathrm{n}\Omega} = \begin{bmatrix} 0 & \dfrac{\partial}{\partial z} & 0 \\ 0 & \dfrac{\partial}{\partial x} & 0 \\ 0 & 0 & 0 \end{bmatrix} \\ \boldsymbol{D}_{\mathrm{n}y} = \begin{bmatrix} 0 & 0 & \dfrac{\partial}{\partial y} \\ \dfrac{\partial}{\partial y} & 0 & 0 \\ 0 & \dfrac{\partial}{\partial y} & 0 \end{bmatrix} \end{cases} \tag{4}$$

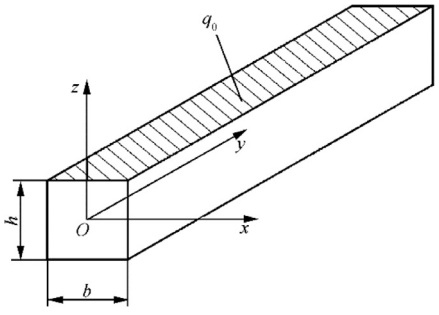

Fig. 1 Coordinate frame of beam model.

The stress components are given by constitutive laws:

$$\boldsymbol{\sigma} = \widetilde{\boldsymbol{C}}\boldsymbol{\varepsilon} \tag{5}$$

where $\boldsymbol{\sigma}$ is the stress vector, $\boldsymbol{\varepsilon}$ is the strain vector and $\widetilde{\boldsymbol{C}}$ is the constitutive matrix. Eq. (5) can be split by using Eq. (2):

$$\begin{cases} \boldsymbol{\sigma}_{\mathrm{p}} = \widetilde{\boldsymbol{C}}_{\mathrm{pp}}\boldsymbol{\varepsilon}_{\mathrm{p}} + \widetilde{\boldsymbol{C}}_{\mathrm{pn}}\boldsymbol{\varepsilon}_{\mathrm{n}} \\ \boldsymbol{\sigma}_{\mathrm{n}} = \widetilde{\boldsymbol{C}}_{\mathrm{np}}\boldsymbol{\varepsilon}_{\mathrm{p}} + \widetilde{\boldsymbol{C}}_{\mathrm{nn}}\boldsymbol{\varepsilon}_{\mathrm{n}} \end{cases} \tag{6}$$

In the case of an isotropic material, the matrices $\widetilde{\boldsymbol{C}}_{\mathrm{pp}}$, $\widetilde{\boldsymbol{C}}_{\mathrm{pn}}$, $\widetilde{\boldsymbol{C}}_{\mathrm{np}}$, and $\widetilde{\boldsymbol{C}}_{\mathrm{nn}}$ are given by

$$\begin{cases} \widetilde{\boldsymbol{C}}_{\mathrm{pp}} = \begin{bmatrix} \widetilde{C}_{11} & \widetilde{C}_{12} & 0 \\ \widetilde{C}_{12} & \widetilde{C}_{22} & 0 \\ 0 & 0 & \widetilde{C}_{44} \end{bmatrix} \\ \widetilde{\boldsymbol{C}}_{\mathrm{nn}} = \begin{bmatrix} \widetilde{C}_{55} & 0 & 0 \\ 0 & \widetilde{C}_{66} & 0 \\ 0 & 0 & \widetilde{C}_{33} \end{bmatrix} \\ \widetilde{\boldsymbol{C}}_{\mathrm{pn}} = \widetilde{\boldsymbol{C}}_{\mathrm{np}}^{\mathrm{T}} = \begin{bmatrix} 0 & 0 & \widetilde{C}_{13} \\ 0 & 0 & \widetilde{C}_{23} \\ 0 & 0 & 0 \end{bmatrix} \end{cases} \tag{7}$$

The coefficients $\widetilde{C}_{ij}$ depend on the material properties. They can be derived from the generic case of an orthotropic material.[64]

2.2. Displacement field

The displacement field is expressed within the framework of CUF:

$$\boldsymbol{u}(x,y,z) = F_\tau(x,z)\boldsymbol{u}_\tau(y) \qquad \tau = 1,2,\ldots,M \tag{8}$$

where F_τ are the functions of coordinates x and z on the cross-section, M stands for the number of terms used in the expansion, $\boldsymbol{u}_\tau$ is the vector of the generalized displacements, and the repeated subscript " τ " indicates summation. A Taylor-type expansion is used to determine the functions F_τ, consisting of a MacLaurin series that uses the 2D polynomials $x^i z^j$ as a base. Table 1 presents M and F_τ as functions of the expansion order N.

For example, the displacement field of the second-order ($N = 2$) Taylor-type expansion model can be expressed as

$$\begin{cases} u_x = u_{x_1} + xu_{x_2} + zu_{x_3} + x^2u_{x_4} + xzu_{x_5} + z^2u_{x_6} \\ u_y = u_{y_1} + xu_{y_2} + zu_{y_3} + x^2u_{y_4} + xzu_{y_5} + z^2u_{y_6} \\ u_z = u_{z_1} + xu_{z_2} + zu_{z_3} + x^2u_{z_4} + xzu_{z_5} + z^2u_{z_6} \end{cases} \tag{9}$$

Table 1 MacLaurin's polynomials.

Expansion order	M	F_τ
0	1	$F_1 = 1$
1	3	$F_2 = x$, $F_3 = z$
2	6	$F_4 = x^2$, $F_5 = xz$, $F_6 = z^2$
3	10	$F_7 = x^3$, $F_8 = x^2z$, $F_9 = xz^2$, $F_{10} = z^3$
⋮	⋮	⋮
N	$\frac{(N+1)(N+2)}{2}$	$F_{(N^2+N+2)/2} = x^N$, $F_{(N^2+N+4)/2} = x^{N-1}z, \ldots,$ $F_{N(N+3)/2} = xz^{N-1}$, $F_{(N+1)(N+2)/2} = z^N$

Classical beam theories can be obtained as a special case of the generalized formulation. For example, the Timoshenko beam theory is obtained in two steps: (a) a first-order displacement field is considered:

$$\begin{cases} u_x = u_{x_1} + xu_{x_2} + zu_{x_3} \\ u_y = u_{y_1} + xu_{y_2} + zu_{y_3} \\ u_z = u_{z_1} + xu_{z_2} + zu_{z_3} \end{cases} \tag{10}$$

and (b) the displacements u_x and u_z must be constant in the cross-section:

$$u_{x_2} = u_{x_3} = u_{z_2} = u_{z_3} = 0 \tag{11}$$

2.3. Principle of virtual work

The static version of the principle of virtual work is applied:

$$\delta L_{\mathrm{int}} = \int_V (\delta\boldsymbol{\varepsilon}_{\mathrm{p}}^{\mathrm{T}}\boldsymbol{\sigma}_{\mathrm{p}} + \delta\boldsymbol{\varepsilon}_{\mathrm{n}}^{\mathrm{T}}\boldsymbol{\sigma}_{\mathrm{n}})\mathrm{d}V = \delta L_{\mathrm{ext}} \tag{12}$$

where δ stands for the virtual variation operator, L_{int} stands for the strain energy, and L_{ext} is the external work. Substituting Eqs. (3), (4), and (6) in Eq. (12), the following expression is obtained:

$$\begin{aligned} \delta L_{\mathrm{int}} = \int_y \int_\Omega \Big\{ & [\boldsymbol{D}_{\mathrm{p}}\delta\boldsymbol{u}]^{\mathrm{T}}[\widetilde{\boldsymbol{C}}_{\mathrm{pp}}\boldsymbol{D}_{\mathrm{p}} + \widetilde{\boldsymbol{C}}_{\mathrm{pn}}(\boldsymbol{D}_{\mathrm{n}\Omega} + \boldsymbol{D}_{\mathrm{ny}})]\boldsymbol{u} \\ & + [(\boldsymbol{D}_{\mathrm{n}\Omega} + \boldsymbol{D}_{\mathrm{ny}})\delta\boldsymbol{u}]^{\mathrm{T}}[\widetilde{\boldsymbol{C}}_{\mathrm{np}}\boldsymbol{D}_{\mathrm{p}} + \widetilde{\boldsymbol{C}}_{\mathrm{nn}}(\boldsymbol{D}_{\mathrm{n}\Omega} + \boldsymbol{D}_{\mathrm{ny}})]\boldsymbol{u} \Big\}\mathrm{d}\Omega\mathrm{d}y \\ = & \ \delta L_{\mathrm{ext}} \end{aligned} \tag{13}$$

Substituting Eqs. (4), (7), and (8) in Eq. (13) and integrating by parts results in the following:

$$\delta L_{\mathrm{int}} = \int_y \delta\boldsymbol{u}_s^{\mathrm{T}}\boldsymbol{K}^{\tau s}\boldsymbol{u}_\tau\mathrm{d}y + [\delta\boldsymbol{u}_s^{\mathrm{T}}\boldsymbol{\Pi}^{\tau s}\boldsymbol{u}_\tau]_{y=0}^{y=L} = \delta L_{\mathrm{ext}} \tag{14}$$

where $\boldsymbol{K}^{\tau s}$ is the stiffness matrix and $\boldsymbol{\Pi}^{\tau s}$ is the matrix of the natural boundary conditions. The components of $\boldsymbol{K}^{\tau s}$ are provided as

$$\begin{cases} K^{\tau s}_{(11)} = E^{22}_{\tau_{,x}s_{,x}} + E^{44}_{\tau_{,z}s_{,z}} - E^{66}_{\tau s}\frac{\partial^2}{\partial y^2}, \ K^{\tau s}_{(12)} = E^{23}_{\tau_{,x}s}\frac{\partial}{\partial y} - E^{66}_{\tau s_{,x}}\frac{\partial}{\partial y}, \\ K^{\tau s}_{(13)} = E^{12}_{\tau_{,x}s_{,z}} + E^{44}_{\tau_{,z}s_{,x}} \\ K^{\tau s}_{(21)} = E^{66}_{\tau_{,x}s}\frac{\partial}{\partial y} - E^{23}_{\tau s_{,x}}\frac{\partial}{\partial y}, \ K^{\tau s}_{(22)} = E^{55}_{\tau_{,z}s_{,z}} + E^{66}_{\tau_{,x}s_{,x}} - E^{33}_{\tau s}\frac{\partial^2}{\partial y^2}, \\ K^{\tau s}_{(23)} = E^{55}_{\tau_{,z}s}\frac{\partial}{\partial y} - E^{13}_{\tau s_{,z}}\frac{\partial}{\partial y} \\ K^{\tau s}_{(31)} = E^{12}_{\tau_{,z}s_{,x}} + E^{44}_{\tau_{,x}s_{,z}}, \ K^{\tau s}_{(32)} = E^{13}_{\tau_{,z}s}\frac{\partial}{\partial y} - E^{55}_{\tau s_{,z}}\frac{\partial}{\partial y}, \\ K^{\tau s}_{(33)} = E^{11}_{\tau_{,z}s_{,z}} + E^{44}_{\tau_{,x}s_{,x}} - E^{55}_{\tau s}\frac{\partial^2}{\partial y^2} \end{cases} \tag{15}$$

where a cross-sectional moment parameter has been used, and a generic term is defined as

$$E^{\alpha\beta}_{\tau_{,\gamma}s_{,\theta}} = \int_\Omega \widetilde{C}_{\alpha\beta}F_{\tau,\gamma}F_{s,\theta}\mathrm{d}\Omega \tag{16}$$

The suffix after the comma denotes the derivatives. The components of $\boldsymbol{\Pi}^{\tau s}$ are provided as follows:

$$\begin{cases} \Pi^{\tau s}_{(11)} = E^{66}_{\tau s}\dfrac{\partial}{\partial y}, \Pi^{\tau s}_{(12)} = E^{66}_{\tau s_{,x}}, \Pi^{\tau s}_{(13)} = 0 \\ \Pi^{\tau s}_{(21)} = E^{23}_{\tau s_{,x}}, \Pi^{\tau s}_{(22)} = E^{33}_{\tau s}\dfrac{\partial}{\partial y}, \Pi^{\tau s}_{(23)} = E^{13}_{\tau s_{,z}} \\ \Pi^{\tau s}_{(31)} = 0, \Pi^{\tau s}_{(32)} = E^{55}_{\tau s_{,z}}, \Pi^{\tau s}_{(33)} = E^{55}_{\tau s}\dfrac{\partial}{\partial y} \end{cases} \tag{17}$$

Letting $\boldsymbol{P}_\tau = [\,P_{x\tau} \quad P_{y\tau} \quad P_{z\tau}\,]^{\mathrm{T}}$ define a vector of the generalized forces, the natural boundary conditions can be obtained by substituting Eq. (17) in Eq. (14):

$$\delta u_{xs}: \quad P_{x\tau} = E^{66}_{\tau s} u_{x\tau,y} + E^{66}_{\tau s_{,x}} u_{y\tau} \tag{18a}$$

$$\delta u_{ys}: \quad P_{y\tau} = E^{23}_{\tau s_{,x}} u_{x\tau} + E^{33}_{\tau s} u_{y\tau,y} + E^{13}_{\tau s_{,z}} u_{z\tau} \tag{18b}$$

$$\delta u_{zs}: \quad P_{z\tau} = E^{55}_{\tau s_{,z}} u_{y\tau} + E^{55}_{\tau s} u_{z\tau,y} \tag{18c}$$

2.4. Boundary discontinuous solution

Geometric boundary conditions for simply supported beams, in terms of the displacement variables given in Eq. (8), are expressed as

$$\begin{cases} u_{x\tau}(0) = u_{y\tau,y}(0) = u_{z\tau}(0) = 0 \\ u_{x\tau}(L) = u_{y\tau,y}(L) = u_{z\tau}(L) = 0 \end{cases} \tag{19}$$

Geometric boundary conditions for clamped-clamped beams, in terms of the displacement variables given in Eq. (8), are additional constraints to those given in Eq. (19), which are given as

$$u_{y\tau}(0) = 0 \tag{20a}$$

$$u_{y\tau}(L) = 0 \tag{20b}$$

The displacement variables are assumed as follows:

$$u_{x\tau} = \sum_{m=1}^{p} U_{x\tau m} \sin(\alpha_m y) \qquad 0 \leqslant y \leqslant L \tag{21a}$$

$$u_{y\tau} = \sum_{m=0}^{p} U_{y\tau m} \cos(\alpha_m y) \qquad 0 < y < L \tag{21b}$$

$$u_{z\tau} = \sum_{m=1}^{p} U_{z\tau m} \sin(\alpha_m y) \qquad 0 \leqslant y \leqslant L \tag{21c}$$

where m is the wave number of the trigonometric term and p is the number of trigonometric terms of the series. The coefficient α_m is given by

$$\alpha_m = \frac{m\pi}{L} \tag{22}$$

The total number of unknown Fourier coefficients introduced in Eq. (21) is $M(3p+1)$. The assumed solution satisfies the simply supported geometric boundary conditions given in Eq. (19). However, the clamped support boundary condition, given in Eq. (20), is not satisfied. In order to obtain an analytical solution for clamped beams, the boundary discontinuous method is used. The details of the procedure are given in Refs.[37,38]

The boundary discontinuous method introduces boundary Fourier coefficients arising from discontinuities of a solution at the edges $y = 0, L$. The displacement variable $u_{y\tau}$ as given by Eq. (21b) does not satisfy the boundary condition for clamped supports given in Eq. (20). Therefore, it is forced to vanish at these edges. The partial derivative $u_{y\tau,y}$ is seen to vanish at the edges, thus violating the complementary boundary constraint or boundary discontinuities at these edges; see Refs.[37,38] For further differentiation, $u_{y\tau,yy}$ is expanded in a Fourier series in order to satisfy the complementary boundary constraint. It is important to note that the derivative of the Fourier series of a given function is not necessarily the same as the Fourier series of the derivative of the function when this function has discontinuities.

The Fourier series of the derivative $u_{y\tau,y}$ is given by

$$u_{y\tau,y} = \sum_{m=1}^{p} U_{y\tau m,y} \sin(\alpha_m y) \quad 0 < y < L \tag{23a}$$

$$U_{y\tau m,y} = \frac{2}{L} \int_0^L u_{y\tau,y} \sin(\alpha_m y) \mathrm{d}y \tag{23b}$$

where $U_{y\tau m,y}$ is the Fourier term associated with the Fourier series of the function $u_{y\tau,y}$. Integrating Eq. (23b) by parts and using the vanishing boundary conditions given in Eq. (20) obtains:

$$\begin{cases} U_{y\tau m,y} = \dfrac{2}{L} u_{y\tau} \sin(\alpha_m y)\big|_{y=0}^{y=L} - \dfrac{2}{L} \displaystyle\int_0^L u_{y\tau} \alpha_m \cos(\alpha_m y) \mathrm{d}y \\ U_{y\tau m,y} = -\alpha_m \dfrac{2}{L} \displaystyle\int_0^L u_{y\tau} \cos(\alpha_m y) \mathrm{d}y \end{cases} \tag{24}$$

The Fourier term $U_{y\tau m}$ of the Fourier series of the function $u_{y\tau}$ is recognized:

$$U_{y\tau m,y} = -\alpha_m U_{y\tau m} \tag{25}$$

Thus, the first derivative can be obtained through term-by-term differentiation. However, it will be demonstrated that the second derivative has a different form. The Fourier series of the second derivative $u_{y\tau,yy}$ is given by

$$u_{y\tau,yy} = \frac{1}{2} a_\tau + \sum_{m=1}^{p} U_{y\tau m,yy} \cos(\alpha_m y) \quad 0 < y < L \tag{26a}$$

$$U_{y\tau m,yy} = \frac{2}{L} \int_0^L u_{y\tau,yy} \cos(\alpha_m y) \mathrm{d}y \tag{26b}$$

where $U_{y\tau m,yy}$ is the Fourier term of the function $u_{y\tau,yy}$ and a_τ is a Fourier coefficient. Integrating Eq. (26b) by parts obtains:

$$U_{y\tau m,yy} = \frac{2}{L} u_{y\tau,y} \cos(\alpha_m y)\big|_{y=0}^{y=L} + \frac{2}{L} \int_0^L u_{y\tau,y} \alpha_m \sin(\alpha_m y) \mathrm{d}y \tag{27}$$

Note that the function $u_{y\tau,y}$ is not necessarily zero at the edges since discontinuities are introduced at $y = 0, L$ (Eq. (21b) is not valid at the edges). Substituting Eqs. (23b) and (25) in Eq. (27), the Fourier term is obtained as

$$U_{y\tau m,yy} = \frac{2}{L}[(-1)^m u_{y\tau,y}(L) - u_{y\tau,y}(0)] - \alpha_m^2 U_{y\tau m} \tag{28}$$

Substituting Eq. (28) in Eq. (26a) the following expression is obtained:

$$u_{y\tau,yy} = \frac{1}{2} a_\tau + \sum_{m=1}^{p} (-\alpha_m^2 U_{y\tau m} + \gamma_m a_\tau + \psi_m b_\tau) \cos(\alpha_m y) \tag{29}$$

where the Fourier coefficients a_τ and b_τ introduce $2M$ new unknowns, resulting in a total of $M(3p+3)$ unknowns. These coefficients are given by

$$a_\tau = \frac{2}{L}[u_{y\tau,y}(L) - u_{y\tau,y}(0)] \tag{30a}$$

$$b_\tau = -\frac{2}{L}[u_{y\tau,y}(L) + u_{y\tau,y}(0)] \tag{30b}$$

and γ_m, ψ_m are defined as

$$(\gamma_m, \psi_m) = \begin{cases} (1,0) & m = \text{even} \\ (0,1) & m = \text{odd} \end{cases} \tag{31}$$

2.5. Virtual work of load

The external work of a load q_0 applied on the surface $z = h/2$ is given by

$$\delta L_{\text{ext}} = \int_0^L \int_{-b/2}^{b/2} q_0 \delta u_z|_{z=h/2} \mathrm{d}x\mathrm{d}y \tag{32}$$

Substituting Eq. (8) in Eq. (32) obtains:

$$\delta L_{\text{ext}} = \delta u_{zs} \int_0^L \left(\int_{-b/2}^{b/2} q_0 F_{sz}|_{z=h/2} \mathrm{d}x \right) \mathrm{d}y \tag{33}$$

The load is expressed using a Fourier series:

$$\begin{cases} q_0 = \sum_{m=1}^{p} Q_m \sin(\alpha_m y) \\ Q_m = \dfrac{2}{L} \displaystyle\int_0^L q_0 \sin(\alpha_m y) \mathrm{d}y \end{cases} \tag{34}$$

where Q_m is a Fourier coefficient associated with the Fourier series of the load. Other types of loads can be analyzed in a similar manner.[29]

2.6. Governing equations

Substituting Eqs. (21a)–(21c) and their appropriate partial derivatives in Eq. (14), in conjunction with Eqs. (15), (29), (33), and (34), the following expressions are obtained for the case of a beam subjected to a distributed load on the surface $z = h/2$:

$$\sum_{m=1}^{p} \sin(\alpha_m y) \Big\{ (E^{22}_{\tau_{,x}s_{,x}} + E^{44}_{\tau_{,z}s_{,z}} + E^{66}_{\tau s} \alpha_m^2) U_{x\tau m} + (-E^{23}_{\tau_{,x}s} \alpha_m + E^{66}_{\tau s_{,x}} \alpha_m) U_{y\tau m} (E^{12}_{\tau_{,x}s_{,z}} + E^{44}_{\tau_{,z}s_{,x}}) U_{z\tau m} \Big\} = 0 \tag{35a}$$

$$\sum_{m=1}^{p} \cos(\alpha_m y) \Big\{ (E^{66}_{\tau_{,x}s} \alpha_m - E^{23}_{\tau s_{,x}} \alpha_m) U_{x\tau m} + (E^{55}_{\tau_{,z}s_{,z}} + E^{66}_{\tau_{,x}s_{,x}} + E^{33}_{\tau s} \alpha_m^2) U_{y\tau m} (E^{55}_{\tau_{,z}s} \alpha_m - E^{13}_{\tau s_{,z}} \alpha_m) U_{z\tau m} - E^{33}_{\tau s} (\gamma_m a_\tau + \psi_m b_\tau) \Big\} = 0 \tag{35b}$$

$$\sum_{m=1}^{p} \sin(\alpha_m y) \Big\{ (E^{12}_{\tau_{,z}s_{,x}} + E^{44}_{\tau_{,x}s_{,z}}) U_{x\tau m} + (-E^{13}_{\tau_{,z}s} \alpha_m + E^{55}_{\tau s_{,z}} \alpha_m) U_{y\tau m} (E^{11}_{\tau_{,z}s_{,z}} + E^{44}_{\tau_{,x}s_{,x}} + E^{55}_{\tau s} \alpha_m^2) U_{z\tau m} - Q_m \left(\int_{-b/2}^{b/2} F_{\tau z}|_{z=h/2} \mathrm{d}x \right) \Big\} = 0 \tag{35c}$$

$$-E^{33}_{\tau s} \frac{a_\tau}{2} + (E^{55}_{\tau_{,z}s_{,z}} + E^{66}_{\tau_{,x}s_{,x}}) U_{y\tau 0} = 0 \tag{36}$$

Equating the coefficients of the trigonometric functions of Eqs. (35) and (36) to zero yields $M(3p+1)$ linear algebraic equations. Additional equations are supplied by the geometric boundary conditions related to vanishing of the displacement variables $u_{y\tau}$ at the edges $y = 0, L$:

$$u_{y\tau}(0) = 0 \quad \rightarrow \quad \sum_{m=0}^{p} U_{y\tau m} = 0 \tag{37a}$$

$$u_{y\tau}(L) = 0 \quad \rightarrow \quad \sum_{m=0}^{p} (-1)^m U_{y\tau m} = 0 \tag{37b}$$

These equations can be expressed in a more convenient form[58]:

$$U_{y\tau 0} + \sum_{m=2,4}^{p} U_{y\tau m} = 0 \tag{38a}$$

$$\sum_{m=1,3}^{p} U_{y\tau m} = 0 \tag{38b}$$

This step generates $2M$ additional equations, resulting in a total of $M(3p+3)$ linear algebraic equations with as many unknowns.

2.7. Extension to other boundary conditions

In addition to the clamped-clamped boundary condition, the clamped-simple boundary condition can also be analyzed by the present method. A clamped support is considered at $y = 0$ and a simple support at $y = L$. Since the geometric boundary condition given in Eq. (20b) has been relaxed, the function $u_{y\tau}$ is no longer forced to vanish at $y = L$, and Eq. (37b) is no longer required. This step reduces the available equations in M compared to the clamped-clamped case. In addition, discontinuities are no longer introduced at $y = L$, and thus $u_{y\tau,y}$ is equal to zero at this point. By substituting $u_{y\tau,y}(L) = 0$ in Eqs. (30a), (30b), the following relation is obtained:

$$a_\tau = b_\tau \tag{39}$$

This step eliminates M unknowns, and thus the system remains determinate.

3. Numerical results and discussion

The present development has been programmed in MATLAB, and numerical examples are given in the present section. An isotropic square beam, i.e., with $b = h$, is considered in the numerical examples. The displacements, stresses, and geometric parameters are expressed in the following non-dimensional forms:

$$\begin{cases} \bar{\sigma}_{yy} = \dfrac{\sigma_{yy}}{q_0}, \bar{\sigma}_{zz} = \dfrac{\sigma_{zz}}{q_0}, \bar{\sigma}_{yz} = \dfrac{\sigma_{yz}}{q_0}, \bar{\sigma}_{xy} = \dfrac{\sigma_{xy}}{q_0} \\ \bar{u}_z = \dfrac{100 h^3 E}{q_0 L^4} u_z, \bar{u}_y = \dfrac{100 h^3 E}{q_0 L^4} u_y \\ \text{Aspect ratio} = \dfrac{L}{h}, \bar{z} = \dfrac{z}{h} \end{cases} \tag{40}$$

where E is the modulus of elasticity. The Poisson's ratio is considered to be $\nu = 0.3$. The boundary conditions of the beam are indicated by letters C (Clamped support) and S (Simple support).

3.1. Convergence study

A study of the convergence is performed first in order to assess the stability of the results. Fig. 1 shows the geometry of the beam considered. Fig. 2 shows the locations of evaluation points of the studied displacements and stresses.

The beam is subjected to a uniform load q_0 on the surface $z = h/2$. Fig. 3 show the transverse displacement and axial stress of a C-C square beam with $L/h = 10$ as the number of terms in the Fourier series is increased for various expansion orders N. While Navier-type solutions converge quickly and 25 terms are usually sufficient[20], a Fourier series converges slowly if the function has discontinuities. Due to this, the boundary discontinuous method has a slower convergence compared to that of a Navier solution.

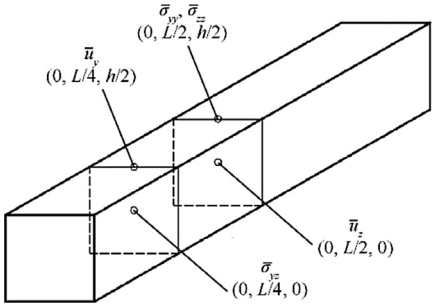

Fig. 2 Location of evaluation points of transverse displacement $\bar{u}_z$, axial stress $\bar{\sigma}_{yy}$, axial displacement $\bar{u}_y$, transverse stress $\bar{\sigma}_{zz}$, and shear stress $\bar{\sigma}_{yz}$.

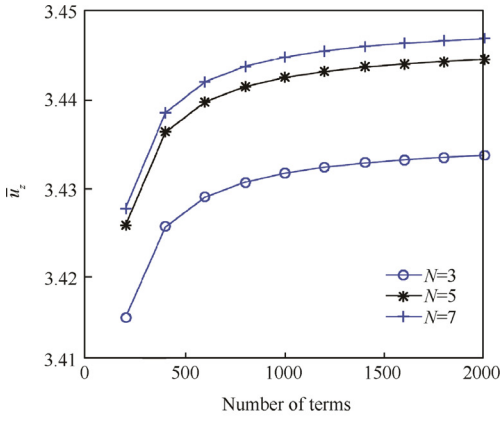

(a) Transverse displacement $\bar{u}_z$ at (0, $L/2$, 0)

(b) Axial stress $\bar{\sigma}_{yy}$ at (0, $L/2$, $h/2$)

Fig. 3 Convergence of transverse displacement $\bar{u}_z$ at (0, $L/2$, 0) and axial stress $\bar{\sigma}_{yy}$ at (0, $L/2$, $h/2$) of a C-C square beam with $L/h = 10$ subjected to a uniform load.

Table 2 presents numerical results for the displacements and stresses as the number of terms in the Fourier series is increased, considering $N = 4$. The transverse stress $\bar{\sigma}_{zz}$ is seen to have a slower convergence. At least 4 significant figures can be expected from the numerical results when the number of terms is $m = 15000$, except for the transverse stress $\bar{\sigma}_{zz}$, and this number of terms is used in the remainder of the manuscript.

3.2. Bending loads

In order to validate the results, a 3D finite element solution of static analysis of the beam has been obtained using ANSYS general purpose program. The 20-noded Solid186 element was used to model the beam, and the mesh was constructed using equally sized cubic elements. In the tables, the 3D finite element solution is denoted by $\text{ANS3D}_{\text{xxx}}$, where the subscript indicates the number of elements in the beam axis. For example, for a beam with $L/h = 5$, the notation ANS3D_{200} stands for a mesh with 200 elements in the beam axis and 40 elements in each axis of the cross-section, resulting in a mesh of $200 \times 40 \times 40$. The error between the results from the present model and the 3D finite element solution (FEM) is defined as

$$\text{Error} = \frac{|\text{Present} - \text{FEM}|}{\text{FEM}} \times 100\% \tag{41}$$

where the most refined finite element mesh solution (i.e. the $\text{ANS3D}_{\text{xxx}}$ model with the largest numerical subscript) is used for calculation of the error

The beam considered and the points of evaluation are the same as those in the previous section, as shown in Figs. 1 and 2. Table 3 presents the values of displacements and stresses at specified points of C-C and C-S square beams with $L/h = 10$, as obtained by the present model, and the corresponding results obtained by the 3D FEM. In order to correctly predict the shear stress $\bar{\sigma}_{yz}$, an expansion order of at least $N = 3$ is required. Very close agreements can be obtained for all the displacements and stresses using an expansion order of $N = 6$ or higher. For higher expansion orders ($N \geqslant 5$), a

Table 2 Convergence of transverse displacement $\bar{u}_z$, axial stress $\bar{\sigma}_{yy}$, transverse normal stress $\bar{\sigma}_{zz}$, axial displacement $\bar{u}_y$, and shear stress $\bar{\sigma}_{yz}$ for a C-C isotropic square beam with $L/h = 10$ subjected to a uniform load.

Number of terms	$\bar{u}_z$	$\bar{\sigma}_{yy}$	$\bar{\sigma}_{zz}$	$\bar{u}_y$	$\bar{\sigma}_{yz}$
400	3.4342	25.406	1.0436	0.46820	3.5096
600	3.4375	25.386	1.0314	0.46853	3.5096
1000	3.4402	25.370	1.0206	0.46879	3.5096
1500	3.4415	25.361	1.0150	0.46892	3.5096
2500	3.4426	25.355	1.0105	0.46902	3.5096
4000	3.4431	25.351	1.0079	0.46908	3.5096
6000	3.4435	25.349	1.0065	0.46911	3.5096
10000	3.4437	25.347	1.0053	0.46914	3.5096
15000	3.4439	25.347	1.0048	0.46915	3.5096

Table 3 Comparison of transverse displacement $\bar{u}_z$, axial stress $\bar{\sigma}_{yy}$, transverse normal stress $\bar{\sigma}_{zz}$, axial displacement $\bar{u}_y$, and shear stress $\bar{\sigma}_{yz}$ for C-C and C-S isotropic square beams with $L/h = 10$ subjected to a uniform load.

Boundary condition	Model		$\bar{u}_z$	$\bar{\sigma}_{yy}$	$\bar{\sigma}_{zz}$	$\bar{u}_y$	$\bar{\sigma}_{yz}$
C-C	FEM	$ANS3D_{340}$	3.4502	25.341	1.0004	0.46907	3.4931
		$ANS3D_{280}$	3.4500	25.340	1.0006	0.46905	3.4939
		$ANS3D_{220}$	3.4497	25.338	1.0010	0.46902	3.4954
	Present	$N = 2$	3.3813 (2.00)	25.034 (1.21)	1.0125 (1.20)	0.46145 (1.63)	2.5000 **(28.43)**
		$N = 3$	3.4355 (0.42)	25.427 (0.34)	1.2627 **(26.22)**	0.46841 (0.14)	3.5096 (0.47)
		$N = 4$	3.4439 (0.18)	25.347 (0.02)	1.0048 (0.43)	0.46915 (0.02)	3.5096 **(0.47)**
		$N = 5$	3.4464 (0.11)	25.321 (0.08)	0.9882 **(1.22)**	0.46874 (0.07)	3.4885 (0.13)
		$N = 6$	3.4479 (0.06)	25.338 (0.01)	1.0027 **(0.23)**	0.46888 (0.04)	3.4885 (0.13)
		$N = 7$	3.4487 (0.04)	25.337 (0.01)	0.9999 **(0.05)**	0.46890 (0.04)	3.4932 (0.00)
C-S	FEM	$ANS3D_{340}$	6.6287	37.909	1.0004	0.85226	5.2319
		$ANS3D_{280}$	6.6285	37.908	1.0006	0.85224	5.2331
		$ANS3D_{220}$	6.6282	37.906	1.0010	0.85221	5.2354
	Present	$N = 2$	6.5478 (1.22)	37.557 (0.93)	1.0122 (1.18)	0.84330 (1.05)	3.7482 **(28.36)**
		$N = 3$	6.6128 (0.24)	37.988 (0.21)	1.2624 **(26.19)**	0.85194 (0.04)	5.2593 (0.52)
		$N = 4$	6.6218 (0.10)	37.911 (0.01)	1.0045 (0.40)	0.85266 (0.05)	5.2577 **(0.49)**
		$N = 5$	6.6246 (0.06)	37.886 (0.06)	0.9878 **(1.26)**	0.85194 (0.04)	5.2258 (0.12)
		$N = 6$	6.6263 (0.04)	37.904 (0.01)	1.0023 **(0.19)**	0.85209 (0.02)	5.2255 (0.12)
		$N = 7$	6.6271 (0.02)	37.904 (0.01)	0.9995 **(0.10)**	0.85208 (0.02)	5.2322 (0.01)

Note: The values in the brackets are the Error (%), and Error = $(|\text{Present} - \text{ANS3D}_{340}|/\text{ANS3D}_{340}) \times 100\%$.

higher reported error is obtained for the transverse stress $\bar{\sigma}_{zz}$; however, for $N = 7$, the higher reported error is around 0.05% and within the margin of error of the 3D FEM solution. Similar trends are observed between the results for C-C and C-S beams.

Fig. 4 show the distributions of the transverse displacement $\bar{u}_z$ across the thickness of C-C and C-S beams with $L/h = 10$, respectively. As the expansion order increases, the results converge to those of the 3D finite element solution in an increasingly slow manner.

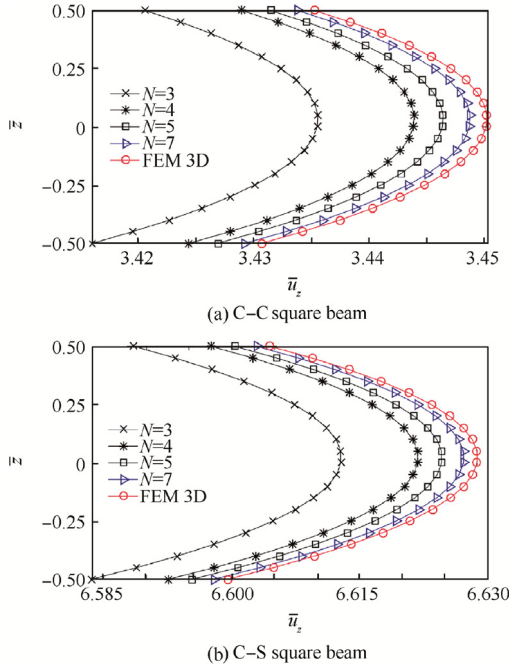

Fig. 4 Distribution of transverse displacement $\bar{u}_z$ at $(0, L/2, z)$ through thickness of C-C and C-S square beams subjected to uniform load with $L/h = 10$.

Fig. 5 shows the distribution of the transverse normal stress $\bar{\sigma}_{zz}$ across the thickness of a C-C beam with $L/h = 10$. An overshoot in the maximum stress is observed for an expansion order of $N = 3$. However, this is corrected by using a higher expansion order. It can be seen that the distributions of the transverse stress across the thickness obtained by using expansion orders of $N = 4$ and $N = 5$ are in close agreements with that of the 3D finite element solution.

Fig. 6 shows the distribution of the shear stress $\bar{\sigma}_{yz}$ across the thickness of a C-C beam with $L/h = 10$. Higher expansion orders are required in order to obtain zero shear stress on the top and bottom surfaces of the beam.

Tables 4 and 5 present the values of displacements and stresses at specified points of C-C and C-S square beams with $L/h = 5$ and 2, respectively. For the critical case of a thick beam with $L/h = 2$, using an expansion order of $N = 7$, the higher reported error is 0.23%.

Fig. 7 shows the distributions of the transverse displacement $\bar{u}_z$ across the thickness of C-C and C-S beams with $L/h = 5$, respectively. Results obtained from higher expansion orders gradually converge to that of the 3D FEM solution, similar to the case with $L/h = 10$.

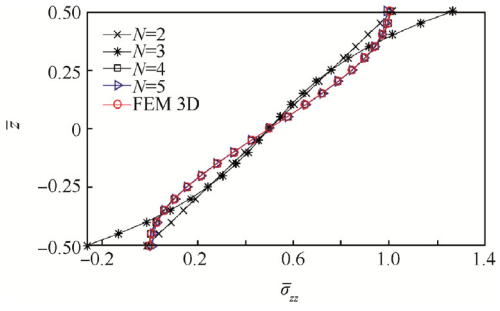

Fig. 5 Distribution of transverse normal stress $\bar{\sigma}_{zz}$ at $(0, L/2, z)$ through thickness of C-C square beam subjected to uniform load with $L/h = 10$.

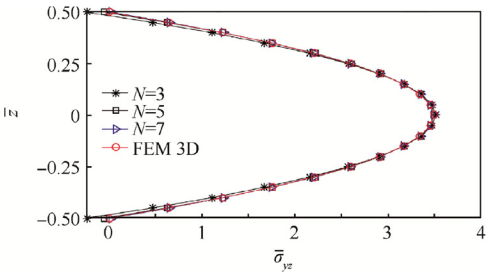

Fig. 6 Distribution of transverse shear stress $\bar{\sigma}_{yz}$ at (0, $L/4$, z) through thickness of C-C square beam subjected to uniform load with $L/h = 10$.

Fig. 8 shows the distribution of the transverse displacement $\bar{u}_z$ across the thickness of a C-C beam with $L/h = 2$. It can be observed that the thickness stretching effect, i.e., variation of the transverse displacement across the thickness, is more pronounced for beams with lower aspect ratios.

3.3. Torsional loads

A beam subjected to two linear loads of equal magnitude q_0 and opposite directions is considered, as shown in Fig. 9. Classic beam models are unable to detect displacement and stresses for this loading case. Table 6 presents results of the shear stress $\bar{\sigma}_{xy}$ evaluated at Point A with coordinates (0, 0,

Table 4 Comparison of transverse displacement $\bar{u}_z$, axial stress $\bar{\sigma}_{yy}$, transverse normal stress $\bar{\sigma}_{zz}$, axial displacement $\bar{u}_y$, and shear stress $\bar{\sigma}_{yz}$ for C-C and C-S isotropic square beams with $L/h = 5$ subjected to uniform load.

Boundary condition	Model		$\bar{u}_z$	$\bar{\sigma}_{yy}$	$\bar{\sigma}_{zz}$	$\bar{u}_y$	$\bar{\sigma}_{yz}$
C-C	FEM	$ANS3D_{200}$	4.5224	6.7009	1.0003	0.96188	1.7507
		$ANS3D_{170}$	4.5221	6.7006	1.0004	0.96183	1.7510
		$ANS3D_{140}$	4.5217	6.7000	1.0006	0.96174	1.7514
	Present	$N = 2$	4.2873 (5.20)	6.4219 (4.16)	1.0117 (1.14)	0.90712 (5.69)	1.2522 **(28.48)**
		$N = 3$	4.4846 (0.84)	6.8092 (1.61)	1.2619 **(26.15)**	0.96112 (0.08)	1.7566 (0.33)
		$N = 4$	4.5062 (0.36)	6.7152 (0.21)	1.0040 (0.37)	0.96467 (0.29)	1.7578 **(0.40)**
		$N = 5$	4.5131 (0.21)	6.6844 (0.25)	0.9871 **(1.32)**	0.96049 (0.14)	1.7481 (0.15)
		$N = 6$	4.5171 (0.12)	6.6994 (0.02)	1.0016 **(0.13)**	0.96116 (0.07)	1.7485 (0.13)
		$N = 7$	4.5190 (0.08)	6.6971 (0.06)	0.9987 **(0.16)**	0.96108 (0.08)	1.7510 (0.01)
C-S	FEM	$ANS3D_{200}$	7.8717	9.9033	1.0003	1.6867	2.5995
		$ANS3D_{170}$	7.8714	9.9030	1.0004	1.6866	2.5998
		$ANS3D_{140}$	7.8709	9.9024	1.0006	1.6865	2.6005
	Present	$N = 2$	7.5936 (3.53)	9.5885 (3.18)	1.0116 (1.13)	1.6205 (3.92)	1.8640 **(28.29)**
		$N = 3$	7.8332 (0.49)	10.0082 (1.06)	1.2618 **(26.14)**	1.6888 (0.13)	2.6111 (0.45)
		$N = 4$	7.8550 (0.21)	9.9160 (0.13)	1.0039 (0.36)	1.6921 (0.32)	2.6112 **(0.45)**
		$N = 5$	7.8622 (0.12)	9.8859 (0.18)	0.9870 **(1.33)**	1.6854 (0.07)	2.5963 (0.12)
		$N = 6$	7.8662 (0.07)	9.9011 (0.02)	1.0015 **(0.12)**	1.6860 (0.04)	2.5965 (0.11)
		$N = 7$	7.8682 (0.05)	9.8989 (0.04)	0.9986 **(0.17)**	1.6858 (0.05)	2.6001 (0.03)

Table 5 Comparison of the transverse displacement $\bar{u}_z$, axial stress $\bar{\sigma}_{yy}$, transverse normal stress $\bar{\sigma}_{zz}$, axial displacement $\bar{u}_y$, and shear stress $\bar{\sigma}_{yz}$ for C-C and C-S isotropic square beams with $L/h = 2$ subjected to a uniform load.

Boundary condition	Model		$\bar{u}_z$	$\bar{\sigma}_{yy}$	$\bar{\sigma}_{zz}$	$\bar{u}_y$	$\bar{\sigma}_{yz}$
C-C	FEM	$ANS3D_{96}$	11.805	1.5332	1.0002	3.0276	0.70624
		$ANS3D_{84}$	11.804	1.5330	1.0003	3.0272	0.70629
		$ANS3D_{72}$	11.802	1.5328	1.0004	3.0268	0.70638
	Present	$N = 2$	10.657 (9.72)	1.2885 (15.96)	1.0381 (3.79)	2.2504 (25.67)	0.50929 **(27.89)**
		$N = 3$	11.609 (1.65)	1.6520 (7.75)	1.2539 **(25.36)**	3.0482 (0.68)	0.70210 (0.59)
		$N = 4$	11.711 (0.80)	1.5495 (1.06)	0.9935 (0.67)	3.1056 **(2.58)**	0.71832 (1.71)
		$N = 5$	11.755 (0.42)	1.5173 (1.04)	0.9868 **(1.34)**	3.0172 (0.34)	0.70666 (0.06)
		$N = 6$	11.778 (0.23)	1.5336 (0.03)	1.0032 **(0.30)**	3.0191 (0.28)	0.70724 (0.14)
		$N = 7$	11.788 (0.14)	1.5306 (0.17)	0.9991 (0.11)	3.0206 **(0.23)**	0.70699 (0.11)
C-S	FEM	$ANS3D_{96}$	16.131	2.0744	1.0002	4.3212	0.98696
		$ANS3D_{84}$	16.130	2.0743	1.0003	4.3208	0.98706
		$ANS3D_{72}$	16.129	2.0741	1.0003	4.3204	0.98721
	Present	$N = 2$	14.772 (8.42)	1.8216 (12.19)	1.0435 (4.33)	3.3495 (22.49)	0.71725 **(27.33)**
		$N = 3$	15.970 (0.99)	2.1934 (5.74)	1.2561 **(25.58)**	4.3790 (1.34)	0.98590 (0.11)
		$N = 4$	16.054 (0.47)	2.0871 (0.61)	0.9903 (0.99)	4.4364 **(2.67)**	1.00363 (1.69)
		$N = 5$	16.090 (0.25)	2.0584 (0.77)	0.9866 **(1.36)**	4.3126 (0.20)	0.98831 (0.14)
		$N = 6$	16.110 (0.13)	2.0756 (0.06)	1.0037 **(0.35)**	4.3131 (0.19)	0.98861 (0.17)
		$N = 7$	16.118 (0.08)	2.0718 (0.13)	0.9988 (0.14)	4.3132 **(0.18)**	0.98827 (0.13)

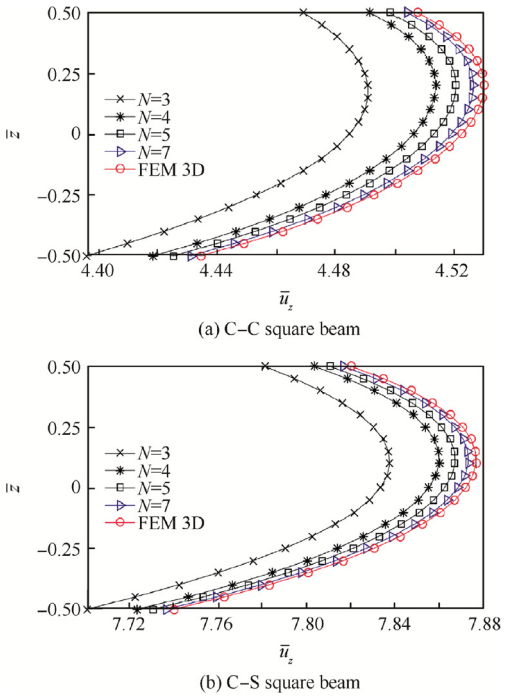

Fig. 7 Distribution of transverse displacement $\bar{u}_z$ at (0, $L/2$, z) through thickness of C-C and C-S square beams subjected to uniform load with $L/h = 5$.

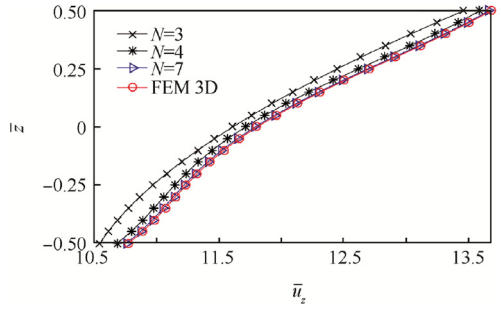

Fig. 8 Distribution of transverse displacement $\bar{u}_z$ at (0, $L/2$, z) through thickness of C-C square beam subjected to uniform load with $L/h = 2$.

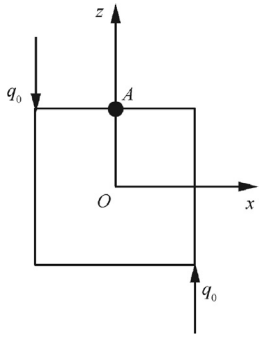

Fig. 9 Geometry of beam subject to torsion loads.

Table 6 Comparison of the shear stress $\bar{\sigma}_{xy}$ for C-C isotropic square beam with $L/h = 2$ subjected to torsional loads.

Model		$\bar{\sigma}_{xy}$	Error (%)
FEM	$ANS3D_{320}$	192.69	
	$ANS3D_{260}$	192.26	
	$ANS3D_{200}$	191.62	
Present	$N = 2$	144.26	25.1
	$N = 3$	145.88	24.3
	$N = 4$	176.32	8.5
	$N = 7$	177.16	8.1
	$N = 8$	179.73	6.7
	$N = 9$	200.17	3.9

$h/2$). It can be observed that higher expansion orders are required in order to correctly predict the shear stress. These results can be used as a benchmark for future finite element works.

4. Conclusions

This paper presents an analytical solution for bending and torsion of a thick rectangular beam with clamped or simple supports. The boundary discontinuous Fourier approach is used in conjunction with shear deformation theories of arbitrary order via Carrera's Unified Formulation (CUF). The important conclusions that emerge from this paper can be summarized as follows:

(1) Accurate analytical results of the stresses and displacements for clamped beams can be obtained by the present model with a low computational effort.
(2) At least an expansion order of $N = 3$ is required in order to correctly predict the maximum shear stress σ_{yz} due to bending loads.
(3) An overshoot of the maximum transverse normal stress σ_{zz} is observed for an expansion order of $N = 3$ when bending loads are considered. However, this is corrected by using higher expansion orders.
(4) The boundary discontinuous method requires a higher computational effort compared to that of Navier-type solutions, but it is much lower than that required for a 3D finite element solution.

Acknowledgment

This paper is dedicated to Professor Reaz Chaudhuri for his outstanding contribution to computational mechanics.

References

1. Kaneko T. On Timoshenko's correction for shear in vibrating beams. *J Phys D: Appl Phys* 1975;**8**(16):1927–36.
2. Hutchinson JR. Transverse vibrations of beams, exact versus approximate solutions. *J Appl Mech* 1981;**48**(4):923–8.
3. Hutchinson JR, Zillmer SD. On the transverse vibration of beams with rectangular cross-section. *J Appl Mech* 1986;**53**(1):39–44.
4. Rychter Z. On the shear coefficient in beam bending. *Mech Res Commun* 1987;**14**(5–6):379–85.

5. Essenburg F. On the significance of the inclusion of transverse normal strain in problems involving beams with surface constraints. *J Appl Mech* 1975;**42**(1):127–32.
6. Levinson M. A new rectangular beam theory. *J Sound Vibrat* 1981;**74**(1):81–7.
7. Rychter Z. On the accuracy of a beam theory. *Mech Res Commun* 1987;**14**(2):99–105.
8. Rychter Z. A simple and accurate beam theory. *Acta Mech* 1988;**75**(1):57–62.
9. Petrolito J. Stiffness analysis of beams using a higher-order beam theory. *Comput Struct* 1995;**55**(1):33–9.
10. Murthy AVK. Towards a consistent beam theory. *AIAA J* 1984;**22**(6):811–6.
11. Bhimaraddi A, Chandrashekhara K. Observations on higher-order beam theory. *J Aerospace Eng* 1993;**6**(4):408–13.
12. Heyliger PR, Reddy JN. A higher order beam finite element for bending and vibration problems. *J Sound Vibrat* 1988;**126**(2):309–26.
13. Kant T, Gupta A. A finite element model for a higher-order shear deformable beam. *J Sound Vibrat* 1988;**125**(2):193–202.
14. Dahake AG, Ghugal YM. A trigonometric shear deformation theory for flexure of thick beam. *Procedia Eng* 2013;**51**:1–7.
15. Khdeir AA, Reddy JN. An exact solution for the bending of thin and thick cross-ply laminated beams. *Compos Struct* 1997;**37**(2):195–203.
16. Sayyad AS, Ghugal YM. Effect of transverse shear and transverse normal strain on bending analysis of cross-ply laminated beams. *Int J Appl Math Mech* 2011;**7**(12):85–118.
17. Shimpi RP, Ghugal YM. A new layerwise trigonometric shear deformation theory for two-layered cross-ply beams. *Compos Sci Technol* 2001;**61**(9):1271–83.
18. Aydogdu M. A new shear deformation theory for laminated composite plates. *Compos Struct* 2009;**89**(1):94–101.
19. Arya H, Shimpi RP, Naik NK. A zigzag model for laminated composite beams. *Compos Struct* 2002;**56**(1):21–4.
20. Mantari JL, Canales FG. A unified quasi-3D HSDT for the bending analysis of laminated beams. *Aerospace Sci Technol* 2016;**54**:267–75.
21. Senjanović I, Vladimir N, Hadžić N, Tomić M. New first order shear deformation beam theory with in-plane shear influence. *Eng Struct* 2016;**110**:169–83.
22. Senjanović I, Vladimir N. Physical insight into Timoshenko beam theory and its modification with extension. *Struct Eng Mech* 2013;**48**(4):519–45.
23. Senjanović I, Rudan S, Vladimir N. Influence of shear on the torsion of thin-walled girders. *Trans FAMENA* 2009;**33**(2):35–50.
24. Senjanović I, Tomašević S, Vladimir N. An advanced theory of thin-walled girders with application to ship vibrations. *Mar Struct* 2009;**22**(3):387–437.
25. Carrera E. Theories and finite elements for multilayered plates and shells: A unified compact formulation with numerical assessment and benchmarking. *Arch Comput Methods Eng* 2003;**10**(3):215–96.
26. Carrera E. Transverse normal strain effects on thermal stress analysis of homogeneous and layered plates. *AIAA J* 2005;**43**(10):2232–42.
27. Carrera E, Boscolo M, Robaldo A. Hierarchic multilayered plate elements for coupled multifield problems of piezoelectric adaptive structures. Formulation and numerical assessment. *Arch Comput Methods Eng* 2007;**14**(4):383–430.
28. Carrera E, Brischetto S, Nali P. Variational statements and computational models for multifield problems and multilayered structures. *Mech Adv Mater Struct* 2008;**15**(3–4):192–8.
29. Carrera E, Giunta G. Refined beam theories based on a unified formulation. *Int J Appl Mech* 2010;**2**(1):117–43.
30. Carrera E, Giunta G, Nali P, Petrolo M. Refined beam elements with arbitrary cross-section geometries. *Comput Struct* 2010;**88**(5–6):283–93.
31. Carrera E, Petrolo M. Refined beam elements with only displacement variables and plate/shell capabilities. *Meccanica* 2012;**47**(3):537–56.
32. Carrera E, Filippi M, Zappino E. Laminated beam analysis by polynomial, trigonometric, exponential and zig-zag theories. *Eur J Mech A/Solids* 2013;**41**:58–69.
33. Catapano A, Giunta G, Belouettar S, Carrera E. Static analysis of laminated beams via a unified formulation. *Compos Struct* 2011;**94**(1):75–83.
34. Giunta G, Biscani F, Belouettar S, Ferreira AJM, Carrera E. Free vibration analysis of composite beams via refined theories. *Compos Part B: Eng* 2013;**44**(1):540–52.
35. Filippi M, Pagani A, Petrolo M, Colonna G, Carrera E. Static and free vibration analysis of laminated beams by refined theory based on Chebyshev polynomials. *Compos Struct* 2015;**132**:1248–59.
36. Ibrahim SM, Carrera E, Petrolo M, Zappino E. Buckling of composite thin walled beams by refined theory. *Compos Struct* 2012;**94**(2):563–70.
37. Chaudhuri RA. On boundary-discontinuous double Fourier series solution to a system of completely coupled P.D.E'.s. *Int J Eng Sci* 1989;**27**(9):1005–22.
38. Chaudhuri RA. On the roles of complementary and admissible boundary constraints in Fourier solutions to the boundary value problems of completely coupled RTH order PDEs. *J Sound Vibrat* 2002;**251**(2):261–313.
39. Chaudhuri RA, Abu-Arja KR. Static analysis of moderately-thick finite antisymmetric angle-ply cylindrical panels and shells. *Int J Solids Struct* 1991;**28**(1):1–15.
40. Kabir HRH, Chaudhuri RA. A direct Fourier approach for the analysis of thin finite-dimensional cylindrical panels. *Comput Struct* 1993;**46**(2):279–87.
41. Chaudhuri RA, Kabir HRH. On analytical solutions to boundary-value problems of doubly-curved moderately-thick orthotropic shells. *Int J Eng Sci* 1989;**27**(11):1325–36.
42. Kabir HRH, Chaudhuri RA. Free vibration of shear-flexible anti-symmetric angle-ply doubly curved panels. *Int J Solids Struct* 1991;**28**(1):17–32.
43. Chaudhuri RA, Kabir HRH. A boundary-continuous-displacement based Fourier analysis of laminated doubly-curved panels using classical shallow shell theories. *Int J Eng Sci* 1992;**30**(11):1647–64.
44. Chaudhuri RA, Kabir HRH. Sensitivity of the response of moderately thick cross-ply doubly-curved panels to lamination and boundary constraint—I. Theory. *Int J Solids Struct* 1993;**30**(2):263–72.
45. Chaudhuri RA, Kabir HRH. Sensitivity of the response of moderately thick cross-ply doubly-curved panels to lamination and boundary constraint—II. Application. *Int J Solids Struct* 1993;**30**(2):273–86.
46. Chaudhuri RA, Kabir HRH. Boundary-discontinuous Fourier analysis of doubly-curved panels using classical shallow shell theories. *Int J Eng Sci* 1993;**31**(11):1551–64.
47. Chaudhuri RA, Kabir HRH. Static and dynamic Fourier analysis of finite cross-ply doubly curved panels using classical shallow shell theories. *Compos Struct* 1994;**28**(1):73–91.
48. Kabir V, Chaudhuri RA. On Gibbs-phenomenon-free Fourier solution for finite shear-flexible laminated clamped curved panel. *Int J Eng Sci* 1994;**32**(3):501–20.
49. Chaudhuri RA, Kabir HRH. A boundary discontinuous Fourier solution for clamped transversely isotropic (pyrolytic graphite) Mindlin plates. *Int J Solids Struct* 1993;**30**(2):287–97.
50. Kabir HRH, Chaudhuri RA. A generalized Navier's approach for solution of clamped moderately-thick cross-ply plates. *Comput Struct* 1991;**17**(4):351–66.
51. Chaudhuri RA, Kabir HRH. Vibration of clamped moderately thick general cross-ply plates using a generalized Navier approach. *Compos Struct* 1993;**24**(4):311–21.

52. Chaudhuri RA. Effect of boundary constraint on the frequency response of moderately thick flat laminated panels. *Compos Eng* 1994;**4**(4):417–28.
53. Kabir HRH. Free vibration of clamped, moderately thick, arbitrarily laminated plates using a generalized Navier's approach. *J Sound Vibrat* 1994;**171**(3):397–410.
54. Chaudhuri RA, Balaraman K, Kunukkasseril VX. A combined theoretical and experimental investigation on free vibration of thin symmetrically laminated anisotropic plates. *Compos Struct* 2005;**67**(1):85–97.
55. Chaudhuri RA, Kabir HRH. Effect of boundary constraint on the frequency response of moderately thick doubly curved cross-ply panels using mixed Fourier solution functions. *J Sound Vibrat* 2005;**283**(1–2):263–93.
56. Kabir HRH, Al-Khaleefi AM, Chaudhuri RA. Frequency response of a moderately thick antisymmetric cross-ply cylindrical panel using mixed type of Fourier solution functions. *J Sound Vibrat* 2003;**259**(4):809–28.
57. Oktem AS, Chaudhuri RA. Fourier solution to a thick cross-ply Levy type clamped plate problem. *Compos Struct* 2007;**79**(4):481–92.
58. Oktem AS, Chaudhuri RA. Boundary discontinuous Fourier analysis of thick cross-ply clamped plates. *Compos Struct* 2007;**82**(4):539–48.
59. Oktem AS, Chaudhuri RA. Effect of inplane boundary constraints on the response of thick general (unsymmetric) cross-ply plates. *Compos Struct* 2008;**83**(1):1–12.
60. Oktem AS, Chaudhuri RA. Sensitivity of the response of thick cross-ply doubly curved panels to edge clamping. *Compos Struct* 2009;**87**(4):293–306.
61. Oktem AS, Chaudhuri RA. Fourier analysis of thick cross-ply Levy type clamped doubly-curved panels. *Compos Struct* 2007;**80**(4):489–503.
62. Oktem AS, Chaudhuri RA. Levy type Fourier analysis of thick cross-ply doubly curved panels. *Compos Struct* 2007;**80**(4):475–88.
63. Oktem AS, Chaudhuri RA. Higher-order theory based boundary-discontinuous Fourier analysis of simply supported thick cross-ply doubly curved panels. *Compos Struct* 2009;**89**(3):448–58.
64. Reddy JN. *Mechanics of laminated composite plates: Theory and analysis*. 2nd ed. Boca Raton: CRC Press; 2004.